601154, 601493, and 601494; T. M. Olson and M. T. Keating, *Trends Cardiovasc. Med.* **7**, 60 (1997); K. R. Bowles *et al.*, *J. Clin. Invest.* **98**, 1355 (1996).
6. Echocardiograms and blood samples for DNA analyses were obtained from participating family members after informed, written consent.
7. The following formulas were used: body surface area (BSA) (m^2) = 0.007184 × height (cm)$^{0.725}$ × weight (kg)$^{0.425}$ [D. Du Bois and E. F. Du Bois, *Arch. Intern. Med.* **17**, 863 (1916)]; 95th percentile for LV end-diastolic dimension (mm) = 45.3 (BSA)$^{1/3}$ − 0.03 (age) − 7.2 + 12% [W. L. Henry, J. M. Gardin, J. H. Ware, *Circulation* **62**, 1054 (1980)]; shortening fraction (%) = 100 × (LV end-diastolic dimension − LV end-systolic dimension) ÷ LV end-diastolic dimension.
8. V. V. Michels, D. J. Driscoll, F. A. Miller, *Am. J. Cardiol.* **55**, 1232 (1985); T. M. Olson and M. T. Keating, *J. Clin. Invest.* **97**, 528 (1996).
9. Hypertrophy of the heart was not evident on electrocardiograms or echocardiograms. Myofibrillar disarray, which is characteristic of hypertrophic cardiomyopathy, was absent on histopathologic examination of cardiac biopsy specimens.
10. I. R. Herman, *Curr. Opin. Cell Biol.* **5**, 48 (1993); M. Gimona, *et al.*, *Cell Motil. Cytoskel.* **27**, 108 (1994); J. Vandekerckhove, G. Bugaisky, M. Buckingham, *J. Biol. Chem.* **261**, 1838 (1986).
11. M.-H. Lu *et al.*, *J. Cell Biol.* **117**, 1007 (1992);
12. Primers were designed according to the published genomic DNA sequence for *ACTC* [H. Hamada, M. G. Petrino, T. Kakunaga, *Proc. Natl. Acad. Sci. U.S.A.* **79**, 5901 (1982)] and OLIGO 4.03 Primer Analysis Software (National Biosciences, Plymouth, MN). The forward primer for exon 5 overlaps 5 base pairs (bp) of coding sequence to avoid a repetitive dinucleotide sequence near the intron-exon boundary. Primer sequences are as follows: exon1F, 5′-CCCCTGAAGCTGTGCCAAGA-3′; exon1R, 5′-GGCTCGGCGGGAAGTTTAC-3′; exon2F, 5′-TAAATGGACAAGACACTGATTAT-3′; exon2R, 5′-CAGCAAGGTCGGTGACTT-3′; exon3F, 5′-GCTAGAGCAGTGGTGTTGTC-3′; exon3R, 5′-AGGTAGGCGGATTCAGTG-3′; exon4F, 5′-CTCACTGAATCCGCCTACCT-3′; exon4R, 5′-CTACACCAGACCCTACAACTC-3′; exon5F, 5′-GACTCGTTCCCAGGTATG-3′; exon5R, 5′-GATCTCCCACTCACAAAAG-3′; exon 6F, 5′-AAGTTTTTGTTTTCTTCTGC-3′; exon 6R, 5′-CATAATACCGTCATCCTGA-3′. Polymerase chain reaction (PCR) product sizes for exons 1 to 6 are 167, 457, 292, 291, 222, and 214 bp, respectively.
13. M. Orita, H. Iwahana, H. Kanazawa, T. Sekiya, *Proc. Natl. Acad. Sci. U.S.A.* **86**, 2766 (1989). PCR was performed with 25 ng of genomic DNA, 10 mM tris-HCL (pH 8.3), 50 mM KCl, 1.5 mM $MgCl_2$, 200 μM deoxyguanosine triphosphate, 200 μM deoxyadenosine triphosphate, 200 μM deoxythymidine triphosphate, 200 μM deoxycytidine triphosphate (dCTP), 0.5 μM forward primer, 0.5 μM reverse primer, 10% glycerol, 0.05 U Taq DNA polymerase, and 1 μCi of [α-^{32}P]dCTP in a final volume of 10 μl. Amplification conditions were 94°C for 5 min, followed by 30 cycles of 94°C for 30 s, 52° to 60°C for 30 s, and 72°C for 30 s followed by 72°C for 10 min (Perkin-Elmer Cetus 9600 thermocycler). For exon 2, 10 μl of PCR product was digested with Bgl II, resulting in 198- and 259-bp fragments. Reactions were diluted with 25 μl of 0.1% SDS, 10 mM EDTA, and 25 μl of 95% formamide dye. Diluted samples were denatured at 94°C for 10 min, and 3-μl samples were subjected to gel electrophoresis under three conditions: 0.5× and 1× Mutation Detection Enhancement gels (FMC Bioproducts, Rockland, ME) at 800 V for 14 to 30 hours (room temperature) and 10% nondenaturing polyacrylamide (49:1 polyacrylamide:bisacrylamide) with 10% glycerol at 30 W for 4 to 6 hours (4°C). Gels were then dried for autoradiography.
14. T. M. Olson *et al.*, data not shown.
15. Normal and anomalous single-strand conformers were cut from dried gels and eluted in 100 μl of water at 65°C for 30 min. The eluted DNA (10 μl) was used as a template for a second PCR with the original primer pair. Products were fractionated in 1% agarose gels and DNA was purified by phenol and chloroform extraction. Forward and reverse [α-^{33}P]-ddNTP (dideoxynucleoside triphosphates) cycle sequencing was performed with a Thermo Sequenase kit (Amersham Life Sciences, Cleveland, OH). Mutations were confirmed by PCR amplification and cycle sequencing of genomic DNA. No additional mutations were identified in other exons of ACTC for either family.
16. Comparison of actin sequences was made by use of the combined protein database and the NCBI BLAST Web site (http://www.ncbi.nlm.nih.gov/cgi-bin/BLAST/nph-blast?form=1).
17. E. S. Hennessey, D. R. Drummond, J. C. Sparrow, *Biochem. J.* **282**, 657 (1993).
18. *Mendelian Inheritance in Man* 102540.
19. K. C. Holmes, D. Popp, W. Gebhard, W. Kabsch, *Nature* **347**, 44 (1990); C. C. Gregorio, *Cell Struct. Funct.* **22**, 191 (1997).
20. B. A. Levine, A. J. G. Moir, V. B. Patchell, S. V. Perry, *FEBS Lett.* **298**, 44 (1992); P. A. Kuhlman, L. Hemmings, D. R. Critchley, *ibid.* **304**, 201 (1992).
21. A. Kumar *et al.*, *Proc. Natl. Acad. Sci. U.S.A.* **94**, 4406 (1997).
22. *Mendelian Inheritance in Man* 302045; R. Oritz-Lopez, H. Li, J. Su, V. Goytia, J. A. Towbin, *Circulation* **95**, 2434 (1997).
23. P. Spirito, C. E. Seidman, W. J. McKenna, B. J. Maron, *N. Engl. J. Med.* **336**, 775 (1997).
24. E. B. Lankford, N. D. Epstein, L. Fananapazir, H. L. Sweeney, *J. Clin. Invest.* **95**, 1409 (1995); H. Watkins, C. E. Seidman, J. G. Seidman, H. S. Feng, H. L. Sweeney, *ibid.* **98**, 2456 (1996).
25. E. Reisler, *Curr. Opin. Cell Biol.* **5**, 41 (1993).
26. L. Mestroni *et al.*, *Br. Heart J.* **72**, S35 (1994).
27. W. Kabsch, H. G. Mannherz, D. Suck, E. F. Pai, K. C. Holmes, *Nature* **347**, 37 (1990). The Insight II molecular modeling system software program (Biosym Technologies, San Diego) was used to create Fig. 3.
28. We thank D. Schaid, F. Miller, D. Driscoll, G. Orsmond, R. Shaddy, and H. Holtzer for support and helpful discussions; W. Edwards (print for Fig. 2); and J. Ross, D. Renlund, J. Mason, J. Anderson, M. Karst, and N. Kishimoto for assistance. Supported by Clinician Scientist Award 96004630 from the American Heart Association (T.M.O.), NIH SCOR grant 5-P50-HL-53773, Project 6 (M.T.K.), the John Patrick Albright Foundation, Public Health Services Research Grant M01-RR00064 from the National Center for Research Resources, and the Technology Access Section of the Utah Genome Center.

3 October 1997; accepted 9 March 1998

Ribonuclease P Protein Structure: Evolutionary Origins in the Translational Apparatus

Travis Stams, S. Niranjanakumari, Carol A. Fierke, David W. Christianson*

The crystal structure of *Bacillus subtilis* ribonuclease P protein is reported at 2.6 angstroms resolution. This protein binds to ribonuclease P RNA to form a ribonucleoprotein holoenzyme with optimal catalytic activity. Mutagenesis and biochemical data indicate that an unusual left-handed βαβ crossover connection and a large central cleft in the protein form conserved RNA binding sites; a metal binding loop may comprise a third RNA binding site. The unusual topology is partly shared with ribosomal protein S5 and the ribosomal translocase elongation factor G, which suggests evolution from a common RNA binding ancestor in the primordial translational apparatus.

Bacterial ribonuclease P (RNase P) is composed of two subunits, an RNA of about 400 nucleotides and a protein of about 120 residues, and the ribonucleoprotein holoenzyme plays a critical supporting role for the translational apparatus by catalyzing the 5′ maturation of pre-tRNA substrates (*1*). Absent the protein subunit, the RNA subunit (RNase P RNA) alone is catalytically active in the presence of elevated salt concentrations and was one of the first ribozymes discovered (*2*). However, the RNase P protein subunit is essential for physiological activity; it decreases the dependence of the reaction on Mg^{2+} concentrations (*2*, *3*), it stabilizes the catalytically active conformation of the RNA subunit (*4*), and it enhances substrate affinity (*5*). The protein subunit also modulates substrate specificity (*6*, *7*). For example, the protein subunit enhances processing of pre-4.5S RNA (*7*), an accessory molecule essential for ribosomal translocation (*8*).

The RNase P ribonucleoprotein holoenzyme (or the RNA subunit by itself) is very much like a classic protein enzyme in that substrate association is mediated by noncovalent interactions (*9*) and multiple turnovers are catalyzed (*2*). Catalysis requires divalent metal ions such as Mg^{2+} or Mn^{2+}, probably to provide nucleophilic metal-bound hydroxide ion for catalysis (*2*, *10*); additionally, at least one metal ion stabilizes the hydrolytic transition state (*11*). Metal ions also stabilize RNA tertiary structure (*3*, *12*) and binding of the pre-tRNA substrate (*11*, *13*). Metal ions increase protein-RNA subunit affinity in the holoenzyme (*14*), but it is not known whether the protein subunit interacts directly with metals. It is interesting to consider that as the protein world evolved from the hypothetical RNA world, metal-dependent ribonucleoproteins such as the RNase P holoen-

T. Stams and D. W. Christianson, Roy and Diana Vagelos Laboratories, Department of Chemistry, University of Pennsylvania, Philadelphia, PA 19104–6323, USA.
S. Niranjanakumari and C. A. Fierke, Department of Biochemistry, Duke University Medical Center, Durham, NC 27710, USA.

*To whom correspondence should be addressed. E-mail: chris@xtal.chem.upenn.edu

zyme may have been common evolutionary intermediates. Consequently, the RNase P protein subunit may have primordial origins early in the evolution of proteins.

To understand RNase P function and evolutionary relationships more clearly, we have determined the x-ray crystal structure of the *Bacillus subtilis* RNase P protein subunit (RNase P protein). Protein was expressed in *Escherichia coli* and purified as described (*5*), and two crystal forms were prepared by the hanging-drop vapor diffusion method (*15*). We determined the structure of RNase P protein in crystal form I by multiple isomorphous replacement with anomalous scattering information at 3.0 Å resolution; it was then refined in crystal form II at 2.6 Å resolution (Table 1). The protein adopts the fold of an α-β sandwich with a globular structure of approximate dimensions 40 × 35 × 30 Å (Fig. 1A). The overall topology is αββββαβα and three likely RNA binding regions are evident, two of which are consistent with available mutagenesis and biochemical data.

The first RNA binding region comprises a highly unusual topological feature: a left-handed βαβ crossover connection from β strand 3 to helix B to β strand 4. This connection violates the empirical rule of right-handed crossover connections between parallel β strands (*16*). Notably, helix B and the preceding loop contain the single ~18-residue consensus sequence conserved among bacterial RNase P proteins (*1*), Lys-Xaa$_{4-5}$-Ala-Xaa$_2$-Arg-Asn-Xaa$_2$-(Lys or Arg)-Arg-Xaa$_2$-(Arg or Lys); we refer to this as the RNR motif (Fig. 1A). Because the unfavorable topology of this conserved motif persisted through evolution, the functional importance of its sequence and structure is amplified. Given the highly basic nature of the RNR motif, it is likely that it is precisely positioned to stabilize binding interactions with RNase P RNA. Helix B packs against helix C at the COOH-terminus of the protein, which contains five exposed basic residues; helix C may similarly interact with RNA.

A second RNA binding region is adjacent to helix B; a large central cleft is formed by helix A and the face of the central β sheet and it is about 20 Å long and 10 Å wide. The base of this cleft contains a row of three exposed aromatic residues, Phe^{16} and Phe^{20} on helix A and Tyr^{34} on β strand 2 (Fig. 1B). Additional residues complete the bottom of the cleft: Ser^{49} on β strand 3, Ile^{86} on β strand 4, and Val^{32} on β strand 2. About 15 arginine and lysine residues surround the cleft. The spliceosomal protein U1A (which has a different overall structure) contains a central cleft of comparable dimensions in which exposed aromatic residues bind single-stranded RNA (*17*). By analogy with U1A, we advance that the central cleft of RNase P protein binds several nucleotides of single-stranded RNA, and exposed aromatic residues may stack with RNA bases.

A third possible RNA binding region is found at one edge of the β sheet, where numerous aspartate and glutamate residues are found in a large polypeptide loop connecting β strands 2 and 3. Because of the highly basic nature of RNase P protein, this

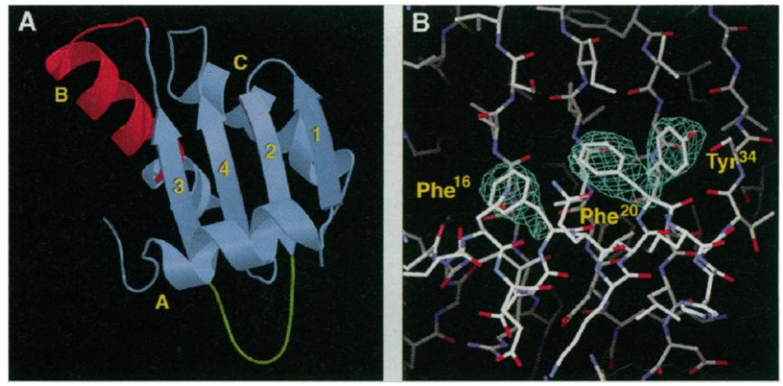

Fig. 1. (**A**) Ribbon plot (*25*) of RNase P protein; α helices and β strands are labeled sequentially by letters and numbers, respectively. The RNR consensus sequence is red, and the carboxylate-rich metal binding loop is green. (**B**) Electron density map of key aromatic residues in the central cleft, generated with Fourier coefficients $|F_o| - |F_c|$ and phases calculated from the final model less the side chain atoms of Phe^{16}, Phe^{20}, and Tyr^{34} (contoured at 3.8σ).

Table 1. Summary of x-ray crystal structure determination. Diffraction data were collected from flash-cooled RNase P protein crystals on an R-AXIS IIc image plate area detector, and intensity data integration and reduction were done with DENZO and SCALEPACK, respectively (*26*). Phases were calculated in crystal form I (space group $P6_3$) by multiple isomorphous replacement (MIR) with anomalous scattering (AS) data from the $SmCl_3$ derivative using the program MLPHARE (*26*). The initial model was fit into a 3.0 Å resolution electron density map calculated with MIR-AS phases solvent-flattened and NCS-averaged with SOLOMON (*26*). This model was then used as a molecular replacement probe and refined against higher resolution data collected at room temperature from crystal form II (space group $P6_4$). Iterative rounds of refinement and rebuilding of the native model were done with X-PLOR and O, respectively (*26*). Individual *B* factors were refined and a bulk solvent correction was applied. Unobserved residues in the final model include Met^1 (>95% cleaved off) and Lys^{115} to Lys^{119} at the COOH-terminus. The final model has excellent stereochemistry, with no residues adopting unfavorable backbone conformations.

Data collection	Native	$SmCl_3$	K_2OsCl_6	Native
Space group	$P6_3$	$P6_3$	$P6_3$	$P6_4$
Resolution (Å)	2.8	3.0	2.8	2.6
Total	17,810	22,694	41,492	15,148
Unique	5,670	4,713	6,200	4,058
Completeness (%)	90.6	91.7	99.7	99.0
R_{merge}*	0.072	0.084	0.087	0.086
Phasing (15 to 3.0 Å)				
Number of sites		1	2	
R_{iso}†		0.351	0.253	
Phasing power‡		0.70	1.37	
Figure of merit (3.0 Å)	0.479			
Refinement statistics (crystal form II, space group $P6_4$)				
Resolution (Å)	20–2.6	R_{cryst}§		0.205
Protein atoms	950	R_{free}§		0.317
Solvent atoms	10	Root mean square deviations		
Zinc ions	2	Bonds (Å)		0.011
Sulfate ions	1	Angles (°)		1.8
Reflections (>3σ)		Dihedrals (°)		25.5
Work	3,361	Impropers (°)		1.5
Test	293			

*$R_{merge} = \Sigma|I_i - \langle I_i\rangle|/\Sigma|\langle I_i\rangle|$, where I_i is the intensity measurement for reflection *i*, and $\langle I_i\rangle$ is the mean intensity calculated for reflection *i* from replicate data. †$R_{iso} = \Sigma||F_{PH}| - |F_P||/\Sigma|F_P|$ calculated for 3.0 Å data, where F_{PH} and F_P are the derivative and native structure factors, respectively. ‡Phasing power = $\langle F_H\rangle/E$ where $\langle F_H\rangle$ is the Rms heavy-atom structure factor and *E* is the residual lack of closure error. §$R = \Sigma||F_o| - |F_c||/\Sigma|F_o|$, where *R* and R_{free} are calculated using the working and test reflection sets, respectively.

clustering of negatively charged residues is surprising. However, two Zn^{2+} ions bind to residues in this loop and mediate interlattice contacts (data not shown); hence, we designate this the metal binding loop (Fig. 1A). Given that protein-RNA affinity increases in the presence of Mg^{2+} (*14*), it is tempting to speculate that Mg^{2+} not only stabilizes RNA conformation (*3*, *12*) but also may associate with the metal binding loop, potentially mediating RNA contacts. Notably, Gln^{38}, Glu^{40}, and a solvent molecule provide one-half of an octahedral Zn^{2+}_A binding site (the other half is provided by their symmetry mates), which is the precise geometry required for Mg^{2+} complexation.

Although molecular details of RNA binding remain to be confirmed by x-ray crystal structure determinations of RNase P protein-RNA complexes, site-directed mutagenesis studies of *E. coli* RNase P protein, named C5 (*18*), illuminate functionally important residues consistent with the first two RNA binding regions observed in the *B. subtilis* RNase P protein structure (Fig. 2). First, substitution of conserved residues in the RNR motif in the left-handed βαβ crossover connection significantly compromises holoenzyme activity and appears to affect substrate specificity. Second, substitution of conserved aromatic residues exposed in the central cleft severely compromises holoenzyme activity, consistent with a possible role in base stacking interactions with RNA.

Photocross-linking studies of *B. subtilis* RNase P protein variants complexed with the RNA subunit and the pre-tRNA substrate (*19*) pinpoint regions of the protein important for RNA binding in the general proximity of functionally important regions identified in C5 mutagenesis studies (*18*) (Fig. 2). Biochemical studies show that RNase P protein interacts with the RNA subunit (*4*, *14*). To date, in preliminary photocross-linking studies with RNase P protein variants labeled with an azidophenacyl moiety at an engineered cysteine residue, protein-RNA cross-links are made between the RNA subunit and either the NH_2-terminus or helix C of the protein (*19*). Intriguingly, a strong photocross-link is observed between pre-$tRNA^{Asp}$ (but not $tRNA^{Asp}$ or the RNA subunit) and azidophenacyl-labeled Ser^{49} → Cys RNase P protein. Although these data must be cautiously interpreted in view of the 10Å length of the cross-linker, they suggest that the central cleft binds the 5′ leader sequence of pre-tRNA in the holoenzyme-substrate complex, possibly accounting for the increased affinity of the holoenzyme toward pre-$tRNA^{Asp}$ relative to $tRNA^{Asp}$ (*5*).

The structure of RNase P protein reveals an unexpected topological relationship with two RNA binding proteins of the translational apparatus despite insignificant sequence identity (<13%): the 70-residue COOH-terminal domain of ribosomal protein S5 (*20*) and the 117-residue domain IV of elongation factor G (EF-G) (*21*, *22*). Even though both proteins lack a counterpart to helix A, and S5 has a β strand 3 so short that it nearly belies formal classification as a secondary structural element, both proteins share a core ββββαβα topology with RNase P protein (Fig. 3). This remarkable structural homology suggests that these proteins evolved from a common ancestor—most likely a primordial ribosomal protein—early in the evolution of the translational apparatus (*22*). Each protein has a left-handed βαβ crossover implicated in RNA binding. The βαβ crossover of RNase P protein contains the base-rich RNR motif, which suggests extensive RNA contacts. The βαβ crossover of S5 contains a critical arginine residue that is believed to interact with 16S RNA (*20*), and the βαβ crossover of EF-G interacts with ribosomal RNA during ribosomal translocation (*21*, *23*). Accordingly, the left-handed βαβ crossover clearly should be considered an established RNA binding element.

In closing, it is instructive to consider how the catalytic function of RNase P is specifically linked with the translocase function of EF-G. The protein subunit of

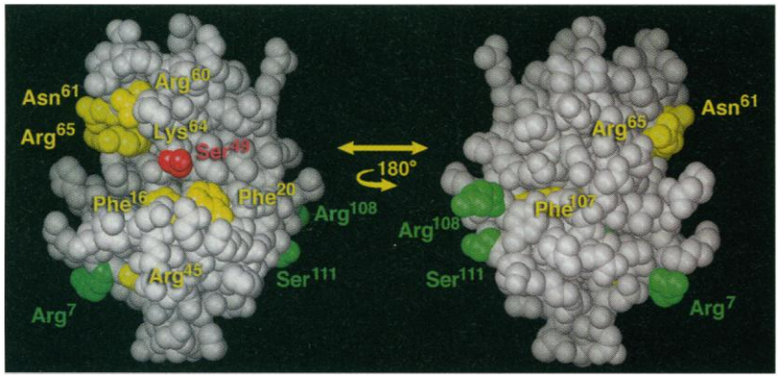

Fig. 2. Space-filling model of *B. subtilis* RNase P protein. Site-directed mutagenesis studies with the *E. coli* C5 protein (*18*) identify residues important for holoenzyme function (yellow); *B. subtilis* numbering is used. Solvent-exposed residues in the central cleft (Phe^{16}, Phe^{20}), on helix B (the RNR motif: Arg^{60}, Asn^{61}, Lys^{64}, Arg^{65}), or on β strand 3 (Arg^{45}) most likely contact RNA. Interestingly, the Arg^{45} → His substitution in C5 protein (*B. subtilis* numbering) results in a temperature-sensitive phenotype defective in holoenzyme assembly (*18*); correspondingly, this substitution must alter a critical contact between the protein and RNA subunits. Substitution of a buried residue (Phe^{107}, which appears as tryptophan in C5 protein) probably slightly perturbs the overall tertiary structure, thereby compromising the overall complementarity of protein and RNA subunits in the holoenzyme. Photocross-linking studies with the *B. subtilis* holoenzyme (*19*) identify residues on the protein subunit that contact the RNA subunit (green), including residues at the NH_2-terminus (Arg^7) and helix C (Arg^{108}, Ser^{111}) that flank helix B. These studies also implicate Ser^{49} (red) and the central cleft for binding the 5′ leader sequence of pre-$tRNA^{Asp}$ in the holoenzyme-substrate complex.

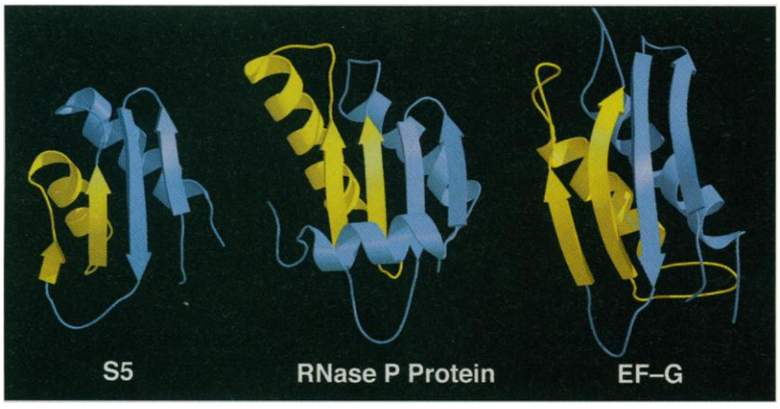

Fig. 3. Ribbon plots (*25*) of the COOH-terminal domain of ribosomal protein S5 (*20*) (PDB accession code 1PKP), RNase P protein, and domain IV of the ribosomal translocase, EF-G (*21*) (PDB accession code 1DAR). Left-handed βαβ crossovers are highlighted in yellow. Topological similarities suggest evolutionary divergence from a primordial ribosomal ancestor.

RNase P plays a critical supporting role for the translational apparatus in *E. coli* by facilitating pre-4.5S RNA processing by the holoenzyme (7). In turn, mature 4.5S RNA binds to the ribosome after translocation and displaces EF-G from the 23S RNA of the large ribosomal subunit before guanosine triphosphate hydrolysis (8). Thus, both the structures and the functions of RNase P protein and EF-G domain IV are specifically linked in the evolution of ribosomal translocation. In view of this relationship, the hypothesis that RNase P protein plays a role in translational autoregulation is rather intriguing (24). With the structure of RNase P protein now in hand, we aim to continue the exploration of structure-function relationships that will illuminate the chemistry and evolutionary biology of RNase P.

REFERENCES AND NOTES

1. S. Altman, *Adv. Enzymol.* **62**, 1 (1989); N. R. Pace and J. W. Brown, *J. Bacteriol.* **177**, 1919 (1995); J. W. Brown, *Nucleic Acids Res.* **26**, 351 (1998).
2. C. Guerrier-Takada, K. Gardiner, T. Marsh, N. Pace, S. Altman, *Cell* **35**, 849 (1983); C. Guerrier-Takada and S. Altman, *Science* **223**, 285 (1984).
3. C. I. Reich, G. J. Olsen, B. Pace, N. R. Pace, *Science* **239**, 178 (1988).
4. S. J. Talbot and S. Altman, *Biochemistry* **33**, 1399 (1994); E. Westhof, D. Wesolowski, S. Altman, *J. Mol. Biol.* **258**, 600 (1996), and references cited therein.
5. J. C. Kurz, S. Niranjanakumari, C. A. Fierke, *Biochemistry* **37**, 2393 (1998).
6. L. A. Kirsebom and S. Altman, *J. Mol. Biol.* **207**, 837 (1989); S. G. Svärd and L. A. Kirsebom, *Nucleic Acids Res.* **21**, 427 (1993); A. Tallsjo and L. A. Kirsebom, *ibid.*, p. 51.
7. A. L. M. Bothwell, R. L. Garber, S. Altman, *J. Biol. Chem.* **251**, 7709 (1976); K. Peck-Miller and S. Altman, *J. Mol. Biol.* **221**, 1 (1991).
8. S. Brown, *Cell* **49**, 825 (1987); *J. Mol. Biol.* **209**, 79 (1989); V. Ribes, K. Römisch, A. Giner, B. Dobberstein, D. Tollervey, *Cell* **63**, 591 (1990).
9. A. Loria and T. Pan, *Biochemistry* **36**, 6317 (1997); L. A. Kirsebom, *Mol. Microbiol.* **17**, 411 (1995), and references cited therein.
10. K. J. Gardiner, T. L. Marsh, N. R. Pace, *J. Biol. Chem.* **260**, 5415 (1985); C. Guerrier-Takada, K. Haydock, L. Allen, S. Altman, *Biochemistry* **25**, 1509 (1986); C. K. Surratt, B. J. Carter, R. C. Payne, S. M. Hecht, *J. Biol. Chem.* **265**, 22513 (1990); J.-P. Perreault and S. Altman, *J. Mol. Biol.* **226**, 389 (1992); *ibid.* **230**, 750 (1993); D. Smith and N. R. Pace, *Biochemistry* **32**, 5273 (1993); T. A. Steitz and J. A. Steitz, *Proc. Natl. Acad. Sci. U.S.A.* **90**, 6498 (1993).
11. J. A. Beebe, J. C. Kurz, C. A. Fierke, *Biochemistry* **35**, 10493 (1996).
12. T. Pan, *ibid.* **34**, 902 (1995).
13. W. D. Hardt, J. Schlegl, V. A. Erdmann, R. K. Hartmann, *Nucleic Acids Res.* **21**, 3521 (1993).
14. S. J. Talbot and S. Altman, *Biochemistry* **33**, 1406 (1994).
15. Crystal form I is obtained by equilibrating 5 μl of protein solution [3 mg of RNase P protein per milliliter, 10 mM tris (pH 8.0)] with 5 μl of precipitant buffer [20% polyethylene glycol (M_r 550) monomethyl ether, 25 mM $ZnSO_4$, 100 mM MES (pH 6.25)] in a hanging drop suspended over a 1-ml reservoir of precipitant buffer at room temperature. Hexagonal plates with approximate dimensions 0.15 × 0.15 × 0.05 mm appear within 3 days, diffract x-rays to 2.8 Å resolution, and belong to space group $P6_3$ (unit cell parameters: $a = b = 85.1$ Å, $c = 60.5$ Å; two molecules in the asymmetric unit). Crystal form II is obtained by equilibrating 5 μl of protein solution [24 mg of RNase P protein per milliliter, 10 mM tris (pH 8.0)] with 5 μl of precipitant buffer [23% polyethylene glycol (M_r 550) monomethyl ether, 10 mM $ZnSO_4$, 100 mM MES (pH 6.5)] in a hanging drop suspended over a 1-ml reservoir of precipitant buffer at room temperature. Crystals with approximate dimensions 0.4 × 0.2 × 0.2 mm appear within 4 days, diffract x-rays to 2.6 Å resolution, and belong to space group $P6_4$ (unit cell parameters: $a = b = 82.4$ Å, $c = 33.5$ Å; one molecule in the asymmetric unit).
16. J. S. Richardson, *Methods Enzymol.* **115**, 341 (1985).
17. C. Oubridge, N. Ito, P. R. Evans, C.-H. Teo, K. Nagai, *Nature* **372**, 432 (1994).
18. M. F. Baer, D. Wesolowski, S. Altman, *J. Bacteriol.* **171**, 6862 (1989); V. Gopalan, A. D. Baxevanis, D. Landsman, S. Altman, *J. Mol. Biol.* **267**, 818 (1997). The RNase P protein from *E. coli* is named C5 and exhibits 29% sequence identity with the *B. subtilis* protein.
19. S. Niranjanakumari and C. A. Fierke, unpublished data. An equimolar concentration of azidophenacyl-labeled RNase P protein was mixed with either RNase P RNA alone {10 nM [^{32}P]RNase P RNA in 5 mM $MgCl_2$, 100 mM NH_4Cl, 20 mM tris (pH 8.0)} or RNase P RNA plus pre-tRNA^{Asp} {400 nM holoenzyme, 5 nM [^{32}P]pre-tRNA^{Asp} in 5 mM $CaCl_2$, 100 mM NH_4Cl, 50 mM MES, 50 mM tris (pH 6.0)} and irradiated at 312 nm with a polystyrene filter for ≤2 min at 4°C. The cross-linked protein-RNA species was identified by SDS–polyacrylamide gel electrophoresis. Cross-links were specific for either RNaseP RNA or pre-tRNA^{Asp}. In control experiments, no cross-links with tRNA^{Asp} or single-stranded RNA (10 to 35 nucleotides) were observed.
20. V. Ramakrishnan and S. W. White, *Nature* **358**, 768 (1992).
21. J. Czworkowski, J. Wang, T. A. Steitz, P. B. Moore, *EMBO J.* **13**, 3661 (1994); A. Ævarsson *et al.*, *ibid.*, p. 3669.
22. The RNase P protein topology is also related to that of the second domain of DNA gyrase B [D. B. Wigley, G. J. Davies, E. J. Dodson, A. Maxwell, G. Dodson, *Nature* **351**, 624 (1991)]. Topological relationships among ribosomal protein S5, EF-G, and DNA gyrase B were first discussed by A. G. Murzin [*Nature Struct. Biol.* **2**, 25 (1995)].
23. P. Nissen *et al.*, *Science* **270**, 1464 (1995); J. Czworkowski and P. B. Moore, *Biochemistry* **36**, 10327 (1997).
24. F. Hansen, E. Hansen, T. Atlung, *Gene* **38**, 85 (1985).
25. Figures 1A and 3 were prepared with MOLSCRIPT [P. Kraulis, *J. Appl. Crystallogr.* **24**, 946 (1991)] and Raster3D [D. J. Bacon and W. F. Anderson, *J. Mol. Graph.* **6**, 219 (1988); E. A. Merritt and M. E. P. Murphy, *Acta Crystallogr.* **D50**, 869 (1994)].
26. DENZO, SCALEPACK, MLPHARE [Z. Otwinowski, in *Proceedings of the CCP4 Study Weekend*, L. Sawyer, N. Issac, S. Borley, Eds. (SERC Daresbury, Daresbury, UK), pp. 56–62 (1993)]; Z. Otwinowski and W. Minor, *Methods Enzymol.* **276**, 307 (1997); Collaborative Computational Project, Number 4, *Acta Crystallogr.* **D50**, 760 (1994)], SOLOMON [J. P. Abrahams and A. G. W. Leslie, *ibid.* **D52**, 30 (1996)], X-PLOR [A. T. Brünger, J. Kuriyan, M. Karplus, *Science* **235**, 458 (1987)], and O [T. A. Jones, J.-Y. Zou, S. W. Cowan, M. Kjeldgaard, *Acta. Crystallogr.* **A47**, 110 (1991)].

27. We thank J. D. Cox, Z. F. Kanyo, J. C. Kurz, C. A. Lesburg, P. B. Moore, and S. W. White for helpful discussions during the course of this investigation. Supported by grant GM55387 from the National Institutes of Health. T.S. was supported by a Lynch Fellowship. Atomic coordinates have been deposited in the Brookhaven Protein Data Bank (accession code 1A6F).

29 January 1998; accepted 11 March 1998